Electro-photocatalytic Fenton Decolorization of Orange G Using Mesoporous TiO$_2$/stainless Steel Mesh Photo-Electrode Prepared by the Sol-Gel Dip-Coating Method

Ervin Nurhayati[1],[**], Hsinju Yang[1,2],[**], Chienhung Chen[1,2], Chingfang Liu[1], Yaju Juang[1], Chihpin Huang[1],[*] and Chi-chang Hu[3]

[1] Institute of Environmental Engineering, National Chiao Tung University (NCTU), Hsinchu, Taiwan 300.
[2] Material and Chemical Research Laboratories, Industrial Technology Research Institute (ITRI), Hsinchu, Taiwan 300
[3] Department of Chemical Engineering, National Tsing Hua University (NTHU), Hsinchu, Taiwan 300
[*]E-mail: cphuang@mail.nctu.edu.tw
[**]The authors contribute equally to this article

A photo-electrochemical process is a powerful and eco-friendly method for treating industrial wastewater. Electro-photocatalytic Fenton (EPF) was employed for orange G decolorization using two kinds of photo-electrodes with TiO$_2$ film-coated stainless steel (SS) mesh. These photo-electrodes are prepared by a dip-coating method from the sol-gel-derived TiO$_2$ sols incorporating with various amounts of P25+TiO$_2$ powders (SGDC method). The single dip-coated electrode with the TiO$_2$ sol containing 50 g/L P25 powders possesses similar crystallinity and decolorization performance to the four repetitive dip-coated electrodes with pure TiO$_2$ sol. The kinetics of orange G decolorization using P25+TiO$_2$ film electrode in photocatalytic (PC), electro-Fenton (EF) and EPF processes followed pseudo first-order kinetics model, and the EPF has the highest reaction rate. The efficiency of orange G decolorization achieves 78% via the EPF reaction for 3 h. The SGDC method using the TiO$_2$ sol containing P25 powders not only enhances the TiO$_2$ coating on the SS substrate, but also produces microcracks in the film, that facilitates the in-situ generation of ferrous ions and further induces the EPF reaction for an effective degradation of organic matter in wastewater.

1. INTRODUCTION

Industrial wastewater contains various kinds of persistent pollutants that may end up polluting environment and put the ecosystem and human at risk. Color caused by dyestuffs in the wastewater

commonly becomes main target of wastewater treatment because its severe environmental problem [1]. Among other types of dye, azo dye is one of the most commonly used in industries, and represents 70% of dye production worldwide [2].

Fenton process is one of the popular advanced oxidation processes (AOPs) in wastewater treatments to treat persistent organics. However, its performance strongly depends on the precise dosing of ferrous sulfate and hydrogen peroxide. In order to sustain the reactions, rendering the traditional Fenton process is unfavorable. Consequently, more efforts have been paid to overcome this drawback using electrochemical processes or the combination of electro-Fenton and photocatalytic processes. This process is known as electrochemical advanced oxidation processes (EAOPs), which have been proved to improve the degradation power of synthetic organic dyes [3].

Compared to the conventional Fenton, the electro-Fenton is a more environmental-friendly process since the reagents required are electro-generated in-situ. As a result, the process can be better controlled and the cost of transporting and storing the chemical reagents can be eliminated [4]. Other than that, using electricity do not cause the generation of secondary pollutants.

The satisfactory results of photoelectron-Fenton application to degrade various chemicals have also been frequently reported [5–8]. Titanium dioxide, the most popular photocatalyst, has been widely employed in various forms as electrodes in photocatalytic and electrochemical applications, such as for water and air purifications [9], water-splitting [10], gas sensors [11], and electrochromic devices [12], because of its high photocatalytic activity and chemical stability under ultraviolet light irradiation.

However, employing TiO_2 nanoparticles in photocatalytic degradation of pollutants has a major disadvantage of separating and recycling the nanoparticles from the treated wastewaters. Therefore, sol-gel and dip-coating (SDGC) is used for the immobilization of TiO_2 nanoparticles on the surface of various substrates, because this techniques is suitable for coating substrates of complex shape [13]. When TiO_2 film is employed as an electro-photocatalyst for degradation of recalcitrant organic pollutants, its electro-photocatalytic activity is significantly affected by the electron/hole pairs separation efficiency [14]. The excellent result achieved by this combined process is a result of the elimination of the electron/hole recombination phenomena. In an electric field, photo-generated electrons can be easily transferred from the TiO_2 film of electrode to the substrate, which hinders the recombination of electron and hole.

The organic degradation/decolorization performances of TiO_2 photo-electrodes in such applications depend on several factors, including the microstructures of TiO_2, applied potential bias, solution pH, and electrolyte conductivity [15]. Among those factors, the microstructure of TiO_2 films can be controlled by varying the preparation parameters and methods. While there are various methods for tuning the microstructure of TiO_2 films [16], the addition of P25 TiO_2 powders to the sol during the sol-gel process for dip-coating TiO_2 films has been reported to be an effective way [17]. The addition of appropriate amount of P25 powders prompts homogenous adhesion, improves mechanical stability and crystallinity, and significantly increases thickness of the resultant films that further enhances their photocatalytic activity compared to TiO_2 film prepared by a conventional SGDC method.

Based on the above reasons, TiO_2 films containing variable amount of P25 TiO_2 were deposited onto the SS mesh substrates via the SGDC method to produce photo-electrodes for the application of wastewater decontamination through EPF process. Several preparation variables in the SDGC method,

such as the surfactant concentration, the dip-coating cycle number, calcination temperature and the P25 TiO_2 loading level, were examined to optimize the EPF performance of the TiO_2/SS photo-electrodes for orange G dye decolorization.

2. MATERIAL AND METHODS

2.1. TiO₂ photo-electrodes preparation

The TiO_2 film was deposited on SS mesh substrates through the SGDC method. All reagents used were of analytical grade. Ethanol, polyethylene glycol (molecular weight 2000, PEG2000), n-butyl alcohol, and inorganic precursors (titanium tetraisopropoxide, TTIP) were purchased from Sigma-Aldrich. Acetyl acetone was purchased from Alfa-Aesar. Different concentrations of PEG2000 ranging from 0.002 to 0.25 M were mixed with n-butyl alcohol (40 mL) and stirred for 30 min. Afterward, 7.22 mL TTIP and 2 mL acetyl acetone were added and stirred at 20 °C for 2 h. Then, 0.72 mL DI water was introduced into the mixture and subsequently stirred for 5 h to obtain the TiO_2 sol. Before TiO_2 deposition, the SS substrates (SUS316, 400 mesh) were immersed in 70% ethanol and 0.93 M H_2SO_4 for 15 and 30 min, respectively, followed by rinsing with DI water. These mesh substrates were then dip-coated with TiO_2 sol and dried at 150 °C for 1 h. This procedure was repeated two or four times to increase the film thickness. After deposition, the film was annealed at 350, 450, 550, and 650 °C for 1 h. For preparing the TiO_2/SS electrodes containing Degussa P25 TiO_2 powders, the pre-treated SS mesh substrates were dip-coated with the TiO_2 sol containing 30, 50 and 70 g/L Degussa P25 TiO_2 powders. The powders were added into the sol at the final step of sol preparation. The SS mesh substrates were dip-coated in this mixture once, dried at 150 °C for 1 h, and then calcined at 550 °C for 1 h. The above photo-electrodes fabricated from the TiO_2 sol without and with 30, 50 and 70 g/L Degussa P25 TiO_2 powders are termed as TiO_2/SS, P25-30+TiO_2/SS, P25-50+TiO_2/SS, and P25-70+TiO_2/SS, respectively.

2.2. Material characterization

The surface morphology and composition of the film were measured by scanning electron microscope (SEM) equipped with an energy dispersive spectrometer (EDS) (Hitachi S-4700I, Japan). The film thickness was obtained by cross-sectional SEM imaging. The crystal structure of the TiO_2 films was analyzed using X-ray diffraction (XRD) (Bruker D2-phaser, USA). The grain size of TiO_2 was calculated by Scherrer's equation based on the full width of half maximum (FWHM) of the anatase peak. N_2 adsorption-desorption experiments were performed on porosity and specific surface area analyzer (Micromeritics Tristar3000, USA) by applying 2-h sample degassing at 200 °C for 2 h before the test. The surface area of the thin film were examined using the Brunauer-Emmett-Teller (BET) method and pore size distribution was calculated according to Barrett-Joyner-Halenda (BJH) formula. The organics residue on TiO_2 film was determined by thermogravimetric analysis (TGA) (Mettler-Toledo 2-HT, USA).

## 2.3. Orange G degradation experiments

The evaluation of all photo-electrodes to decolorize the orange G dye by photocatalysis, electro- and electro-photocatalytic Fenton, was carried out in a batch of two-electrode system. The TiO_2-coated SS mesh electrodes were used as the photo-anode. Meanwhile, the cathode was a graphite sheet (5 cm × 2 cm × 3 mm) in a 100-mL 0.01 M Na_2SO_4 (Merck). The target pollutant was orange G dye at a concentration of 45.2 mg/L. The initial pH was fixed at 3, adjusted by H_2SO_4. The solution was continuously purged by air at a flow rate of 50 mL/min during the decolorization process. The light source for TiO_2 irradiation was a 365 nm UV light (0.2 mW/cm^2). A schematic diagram of the system is shown in Fig.1.

The orange G dye content in the aqueous solutions was measured by UV-vis spectrophotometry (Hitachi U3010 Spectrophotometer, Japan). The decolorization efficiency (E) was determined by Eq. 1:

$$E\% = \frac{(A_0 - A_i)}{A_0} \times 100 \tag{1}$$

where A_i is the intensity of the absorbance of orange G at time i, and A_0 is the initial intensity of the absorbance of orange G. The concentration of ferrous ions in the initial and final solutions was determined using spectrophotometric analysis.
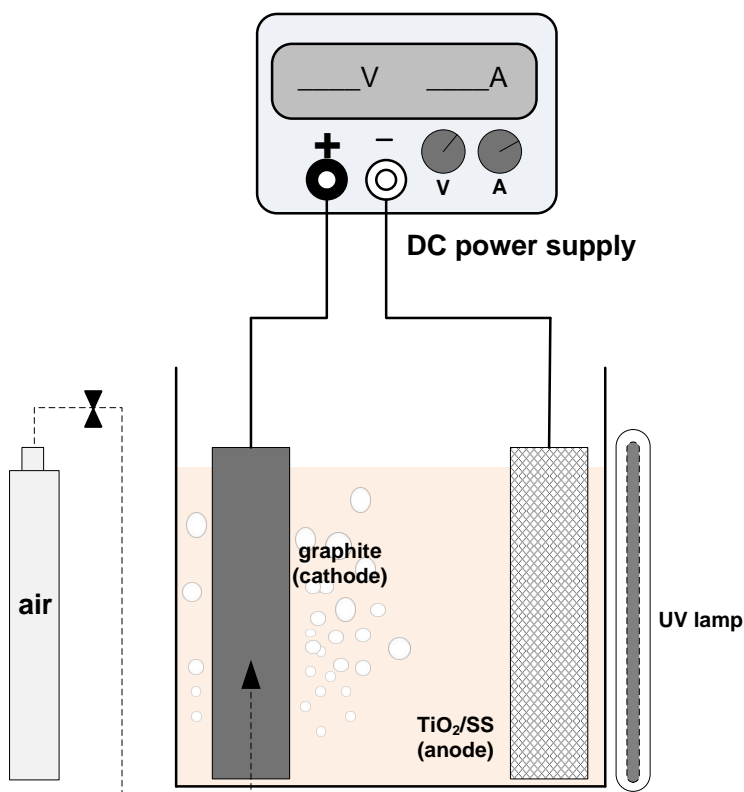
Figure 1. The electro-photocatalytic Fenton system for orange G decolorization.

3. RESULTS AND DISCUSSION

3.1. Effects of the PEG2000 concentration on the microstructure and photocatalytic activity of TiO₂/SS

3.1. Effects of the PEG2000 concentration on the microstructure and photocatalytic activity of TiO_2/SS

The photoactivity of the TiO_2 film depends on the porosity, grain size and phase of the crystallites, surface roughness and surface area [18]. This section discusses the effect of PEG2000 concentration and the number of TiO_2 layer (number of dip-coating cycles) on crystallinity, porosity and surface area of TiO_2/SS as well as on its photocatalytic activity.

The crystallinity of TiO_2 films prepared from the sol solution with variable concentrations of PEG2000 was determined by XRD (see Fig. 2). It shows that increasing the PEG2000 concentration from 60 to 200 mM in the sol-gel process resulted in a higher intensity of anatase (101) peak. However, at concentrations of 2 and 20 mM, the XRD patterns show no diffraction peaks corresponding to the anatase phase, which is attributed to a poor adhesion/coverage of TiO_2. Noted that, addition of PEG2000 into the TiO_2 sol would significantly increase the sol viscosity because of its high molar weight. The viscous sol facilitates the mass loading of TiO_2 on the substrate surface as a consequence of improved adhesion [19], leading to the presence of TiO_2 diffraction peaks. The concentrations of PEG2000 at 2 and 20 mM were too low to assist the attachment of TiO_2 on the SS mesh surface. Hence, no TiO_2 diffraction peaks were observed.

Differing from increasing the PEG2000 concentration, the amount of TiO_2 on the substrate can be increased by repeating the dip-coating process to produce a thick multi-layer film. The thickness of the TiO_2 film on the substrate increased from 1.6 to 7.4 μm when the dip-coating cycle was increased from twice to four times. This is in agreement with previous work [20] where the PEG2000 is one of the effective surfactants for increasing the thickness of film layer.

Other than providing viscosity and adhesion power of the gel, surfactants were also employed as pore-generating/directing agents in the sol-gel method to achieve highly porous TiO_2 films [21]. During the solvent evaporation period, the surfactant molecules in the sol are surrounded by the titania precursor to form mesoscopically ordered inorganic/polymer composites through the self-assembly mechanism [22]. These surfactant molecules are removed subsequently by calcination at high temperatures, resulting in the formation of porous nanocrystalline TiO_2 materials [21].

In this work, nitrogen adsorption-desorption isotherms were measured to assess the porous structure variation of TiO_2 films prepared under different PEG2000 concentrations (Fig. 3). The TiO_2 film without PEG2000 exhibits a non-porous structure according to the Brunauer-Deming-Deming-Teller (BDDT) classification. When 0.06-0.2 M PEG2000 was introduced to the precursor solution, the type IV pore structure with a hysteresis loop was obtained, suggesting the formation of typical materials with bottleneck-shaped pores. For materials with relatively strong interactions between the adsorbed fluid and wall, the type IV adsorption isotherm is commonly found [23]. The hysteresis loop due to the occurrence of capillary condensation [20,23] indicates the mesoporous nature of TiO_2 films. The higher PEG2000 concentration is added, the wider the hysteresis loop is obtained, reflecting the increase in the total pore volume within the film. Furthermore, the dependence of the BET specific surface area and porosity of TiO_2 films on the PEG2000 concentration is given in Table 1. The data

show that the specific surface area and pore volume were increased with the PEG2000 concentration, confirming the role of PEG as a pore generator.
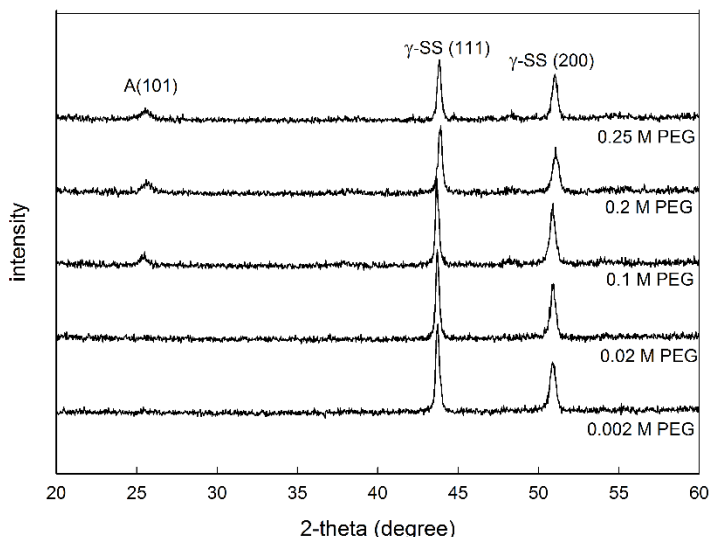
Figure 2. The XRD patterns of TiO$_2$ films prepared with different PEG2000 concentrations of 0.002, 0.02, 0.1, 0.2 and 0.25 M; conditions: two dip-coating cycles and 450 °C calcination for 1 h.
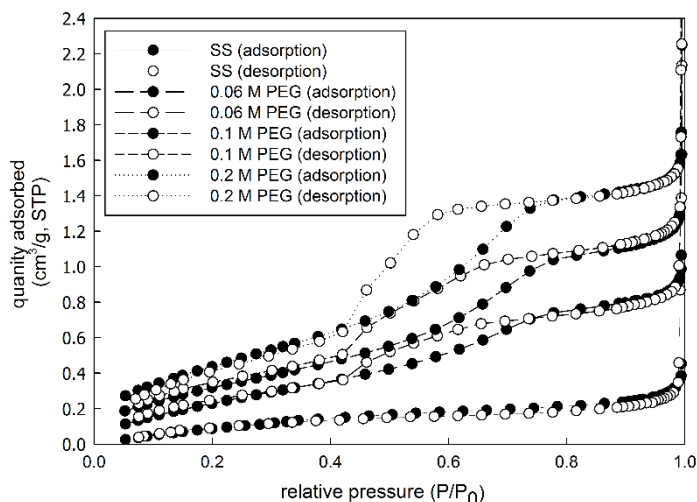

Figure 3. Nitrogen adsorption-desorption isotherms of TiO$_2$ films prepared with different PEG2000 concentrations of 0.06, 0.1, and 0.2 M; conditions: two dip-coating cycles and 450 °C calcination for 1 h.

Table 1. The pore properties of TiO$_2$ films prepared by varying the PEG2000 concentration in the precursor solution.

PEG concentration (M)	BET (m^2/g)	Pore volume (cm^3/g)[a]	Porosity (%)[b]
0	0.56	4.84×10^{-4}	0.19
0.06	1.05	1.74×10^{-3}	0.68
0.1	1.30	2.26×10^{-3}	0.88
0.2	1.62	2.33×10^{-3}	0.91

[a]BJH desorption cumulative volume of pores; [b]Based on pore volume and anatase density of the film (3.9 g/cm^3). (Conditions: 2 dip coating cycles and 450 °C calcination for 1 h)

Increasing porosity of the TiO_2 film by using PEG2000 in the sol-gel method can improve the photoreactivity of TiO_2 film photocatalyst [8]. Figure 4 shows the orange G dye degradation via photocatalytic process by TiO_2/SS-mesh electrode produced with two and four times dip-coating. The decolorization of orange G dye was characterized by the reduction of absorbance of signature peak at the wavelength of 478 nm, which represents the azo-bond (-N=N-) in the structure. With four dip-coating cycles, increasing the PEG concentration from 0.1 to 0.2 M enhanced the decolorization from 8.7 to 13.7% (Fig. 4b), while two dip-coatings showed an insignificant difference with increasing the PEG2000 concentration (Fig. 4a). With the PEG2000 concentration of 0.1 M, increasing the dip-coating cycles from two to four times resulted in an increase of orange G decolorization efficiency from 4.8 to 8.7%. A similar trend was seen when PEG2000 concentration was 0.2 M. The increase of photocatalytic activity is attributed to the thicker film resulting from a four times dip-coating process and more porous film produced by a higher PEG2000 concentration. The relatively low decolorizations of both electrodes suggest that the additional driving force of a combined-system for orange G dye degradation is required to achieve higher efficiency. Therefore, the orange G degradation was operated under electro-photocatalytic Fenton process.


(a)   (b)
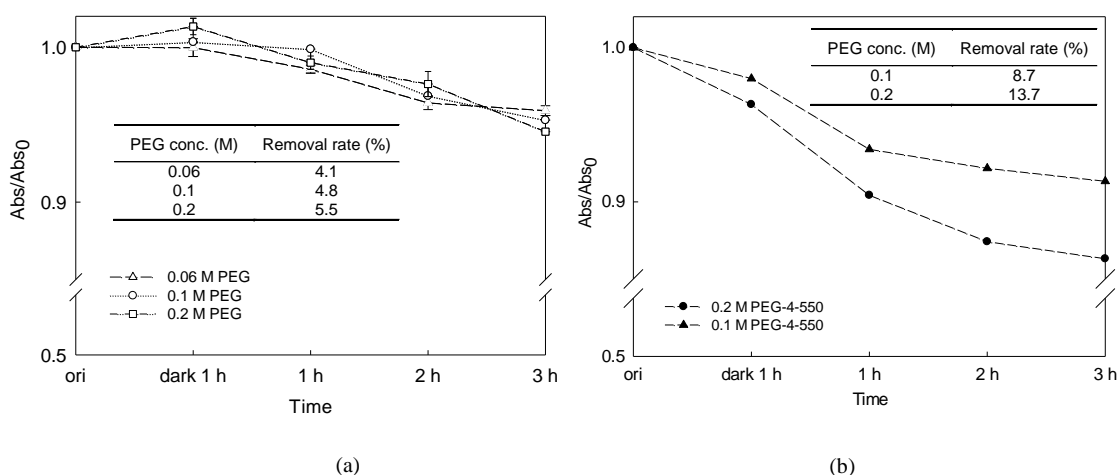
Figure 4. Decolorization efficiency of TiO_2/SS electrode prepared with different PEG2000 concentration and dip-coating times (PEG2000 concentration; dip-coating time): (a) (0.06, 0.1, 0.2 M; twice) and (b) (0.1 and 0.2 M; four times), under photocatalysis process; conditions: orange G dye concentration: 45.2 mg/L, pH: 3, UV light: 0.2 mW/cm^2, Abs. at 478 nm.

3.2. *Effects of the calcination temperature on the microstructure of TiO$_2$/SS*

The SGDC process coupled with the self-assembly method is commonly followed by calcination at high temperatures to remove the soft template molecules and to convert the amorphous film into a nanocrystalline TiO_2 layer. This annealing treatment also improves adhesion of the resultant film on the substrate. However, a too high calcination temperature causes crystallite sintering and pore collapsing, reducing the specific surface area as well as transforming the anatase phase into the rutile structure [17]. All these effects would significantly reduce the photocatalytic activity of TiO_2 films [24].

Figure 5a shows the typical XRD patterns of TiO_2/SS annealed at temperatures ranging from 350 to 650 °C. Clearly, the film annealed at 350 °C of the amorphous structure since no diffraction peak corresponding to the TiO_2 crystal is observed. The peak intensity of (101) anatase phase increases with increasing calcination temperature from 450 to 550 °C. The minor (004), (200), and (211) anatase phases becomes visible when the calcinations temperature equals to 550 °C, suggesting the growth of TiO_2 crystallites. The phase transformation of TiO_2 from anatase to rutile occurs when the temperature is further increased to 650 °C since the rutile phase is a thermodynamically favorable structure. However, not only the crystalline phase of TiO_2, the crystal size is also determined by the temperature as shown in Table 2.
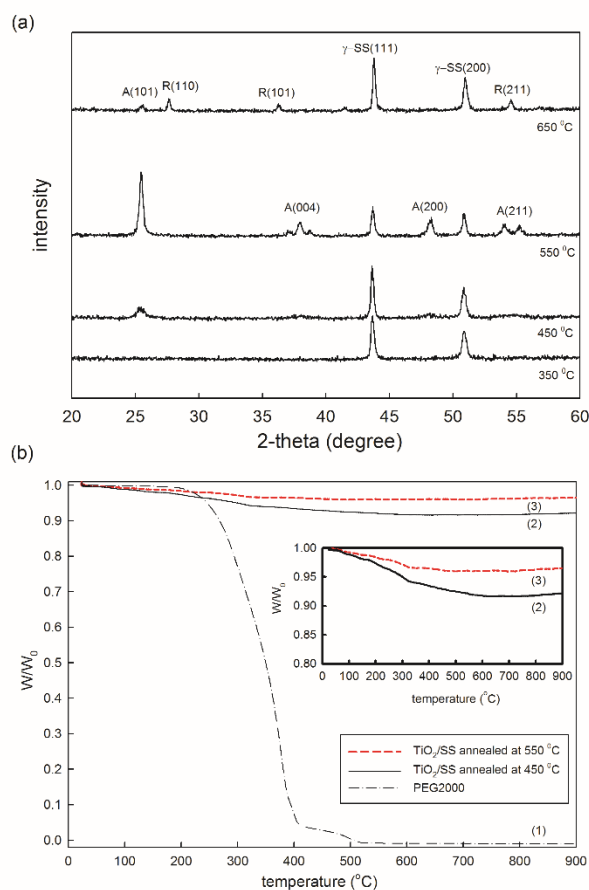
Figure 5. (a) XRD patterns of TiO_2/SS annealed at temperatures of 350–650 °C and (b) TGA curves of (1) PEG2000 and TiO_2/SS annealed at (2) 450 and (3) 550 °C for 1 h; conditions: 4 dip-coating cycles and PEG2000 concentration = 0.2 M.

Figure 5b shows the TGA data of PEG2000 and two TiO_2/SS annealed at 450 and 550 °C. From curve 1, PEG2000 starts to be thermally decomposed at temperature above/equal to 200 °C, and completely decomposed at 500 °C. From a comparison of curves 2 and 3, both electrodes have similar TGA curves which can be separated into three zones. The first zone, from the ambient temperature to about 300 °C, corresponds mainly to the removal of physically adsorbed/chemically bound water. In the second zone from 300 to 550 °C, the gradual loss in mass is caused by the decomposition and evaporation of residual PEG2000 in the TiO_2 film. In the last zone with temperatures above 550 °C, no

significant weight change is observed, suggesting that the residual PEG2000 in the film might be completely removed at temperatures ≥ 550 °C.

Table 2. Crystal size of TiO_2 films prepared with 0.2 M of PEG2000 in the sol at different calcination temperatures.

Temperature (°C)	FWHM (deg)[a]	Crystal size (nm)[b]
450	0.81	10.1
550	0.33	24.4
650	0.19	41.8

[a]The full width of half maximum; [b]Based on anatase (101) XRD patterns calculated using Scherrer's equation [25]
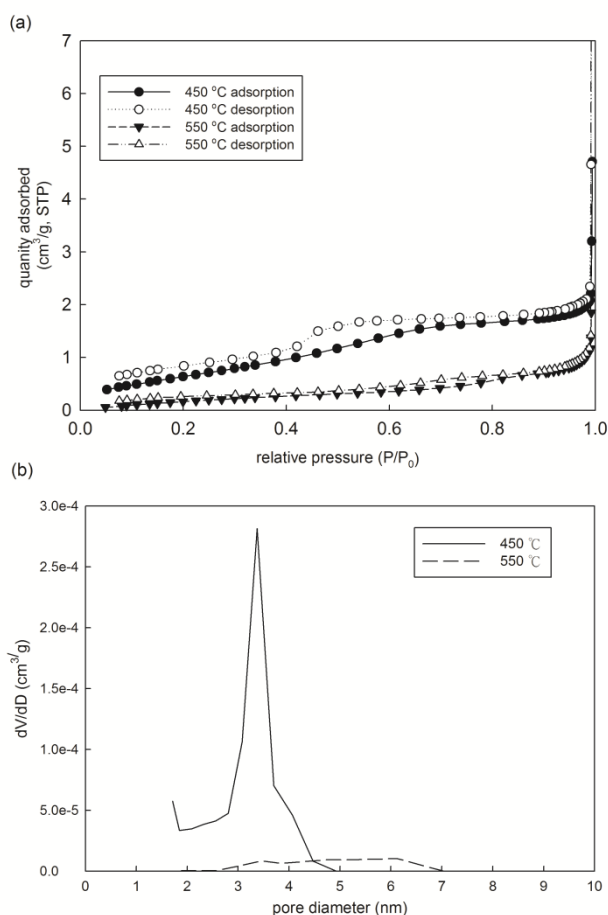
Figure 6. (a) The nitrogen adsorption-desorption isotherms and (b) pore size distribution of TiO_2/SS electrodes annealed at 450 and 550 °C; conditions: 4 dip-coating cycles and PEG2000 concentration = 0.2 M.
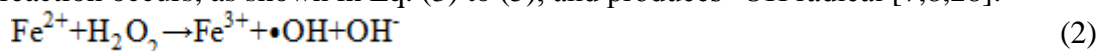
The effect of calcination temperature on the porous structure of TiO_2 films as well as on the pore size distribution was examined. Figure 6a shows the typical N_2 adsorption-desorption isotherms of TiO_2 annealed at 450 and 550 °C, where the adsorption isotherm shows the typical type IV behavior, excepting that these curves are not overlapped in the low relative pressure region. This

indicates the present of residual carbons in the TiO_2 film due to incomplete decomposition of surfactants (Fig. 5b) as a result of the N_2 adsorption-desorption in the low relative pressure region. Furthermore, the pore size distribution of the TiO_2 film annealed at 450 °C (Fig. 6b) shows that the dominant pore diameter is about 3.5 nm. Increasing the calcination temperature to 550 °C causes the pore collapsing, leading to the broad pore size distribution between 3 to 7 nm. A further increase in the calcination temperature to 650 °C consequently induces severe pore collapse, as a result of the internal stresses generated at high temperatures [6].

3.3. Electro-photocatalytic Fenton activity of TiO₂/SS photo-electrodes

The mineralization process of organics present in the water can be accelerated using the photoelectro-Fenton method, where the solution treated under EF conditions is exposed to UV light [8]. Combination of this method with photocatalytic process using TiO_2 further increase the degradation efficiency [26].

The basis of the Fenton oxidation process is the reaction of Fe^{2+} with H_2O_2 to generate •OH that can degrades organic pollutants, as shown in Eq. (2) [27]. In the presence of UV light, a photo-Fenton reaction occurs, as shown in Eq. (3) to (5), and produces •OH radical [7,8,28].

$$Fe^{2+}+H_2O_2 \rightarrow Fe^{3+}+\bullet OH+OH^- \tag{2}$$
$$Fe^{2+}+H_2O_2+h\nu \rightarrow Fe(OH)^{2+}+\bullet OH \tag{3}$$
$$Fe(OH)^{2+}+h\nu \rightarrow Fe^{2+}+\bullet OH \tag{4}$$
$$Fe^{3+}+H_2O_2+h\nu \rightarrow Fe^{2+}+H^++\bullet OH \tag{5}$$

Orange G degradation by photocatalytic oxidation is greatly improved by applying anodic potential bias (photoelectrocatalytic, PEC) [29]. This is due to the elimination of electron/hole recombination since the photogenerated electrons are transported via an external circuit to the counter electrode, avoiding the scavenging effect on the hydroxyl radicals created [26]. Furthermore, by applying graphite as the cathode in present work, electrogenerated H_2O_2 is continuously supplied to the solution by an oxygen reduction reaction on the surface of graphite cathode, as in Eq. (6) [30].

$$O_2+2H^++2e^- \rightarrow 2H_2O_2 \tag{6}$$

The release of iron ions from the SS-mesh substrate served as the electrogenerated iron supply for the Fenton reaction to proceed. Because iron produces bi- and trivalent ions (Fe^{2+} and Fe^{3+}), as shown in equation 7 to 9, the following processes carry out at the anode-solution interface [31].

$$Fe_{(s)} \rightarrow Fe^{2+}_{(aq)}+2e^- \quad Eox_0 = 0.441 \text{ V} \tag{7}$$
$$Fe_{(s)} \rightarrow Fe^{3+}_{(aq)}+3e^- \quad Eox_0 = 0.036 \text{ V} \tag{8}$$
$$Fe^{2+}_{(aq)} \rightarrow Fe^{3+}_{(aq)}+e^- \quad Eox_0 = -0.771 \text{ V} \tag{9}$$

Figure 7 shows the result of applying TiO_2/SS electrode prepared under various calcination temperatures to degrade orange G dye. Other than the UV/vis absorbance at 478 nm, absorbance at 330 nm that is characteristic of naphthalene ring in orange G dye structure, was also monitored. To ensure that Fenton process continued, the ferrous ion content in the solution was also monitored. During the dark reaction no ferrous ions were detected. When applying 1.6 V potential, after the first hour of EPF reaction, the concentrations of ferrous ion in the solution were 0.7, 0.6 and 0.5 mg/L for TiO_2/SS prepared at 450 °C, 550 °C and 650 °C, respectively. The final concentration at the end of the reaction

for both TiO_2/SS prepared at calcination temperature of 450 °C and 550 °C were 1.1 mg/L, while TiO_2/SS-mesh calcined at 650 °C was 0.9 mg/L.
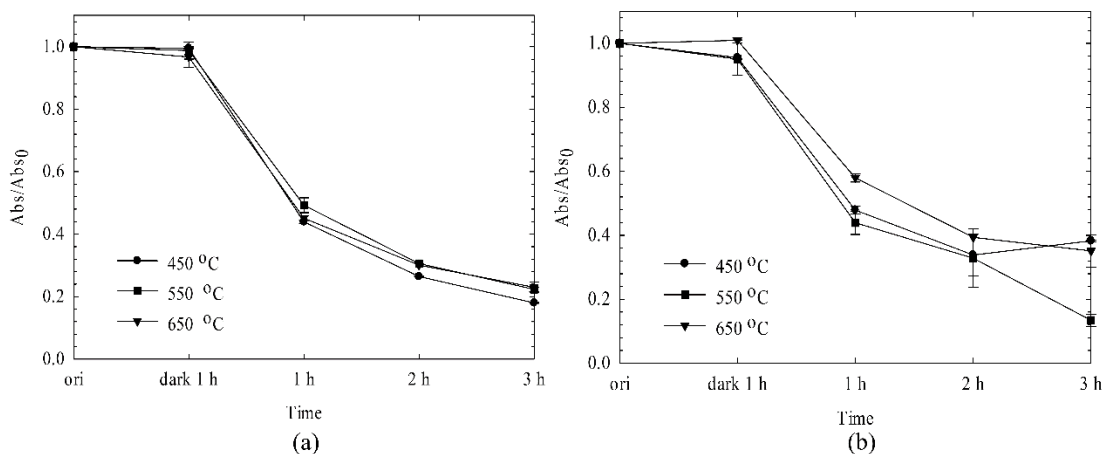
Figure 7. Decolorization efficiency: (a) Abs. at 478 nm (b) Abs. at 330 nm, of TiO_2/SS electrodes prepared at different calcination temperatures of 450–650 °C, under EPF process; conditions: orange G dye concentration: 45.2 mg/L, pH: 3, UV light: 0.2 mW/cm^2, potential applied: 1.6 V.

We observed that the TiO_2/SS electrode did not show any activity with regards to orange G degradation during an hour of dark reaction. In terms of decolorization resulting from the breakage of the -N=N- bond (478 nm), after 3-h of reaction the TiO_2/SS calcined at 450 °C slightly shows a better performance in orange G degradation compared to those calcined at 550 °C and 650 °C (Fig. 7a). This could be related to pore collapse as indicated in Fig. 6b. As for absorbance indicating naphthalene (330 nm), the TiO_2/SS electrode calcined at 550 °C produced the highest removal efficiency (Fig. 7b). The electrode calcined at 450 °C gave a similar result to the one calcined at 550 °C, excepting that after 2 h there was an increase in 330 nm absorbance. This might be caused by the release of residual PEG2000 in the film (Fig. 5b) to the solution. The lowest efficiency for both wavelengths shown by the electrode calcined at 650 °C could be due to the presence of rutile [17].

The two primary phases of titania are rutile (3.0 eV band gap) and anatase (3.2 eV band gap) [32]. With a lower band gap, rutile can be excited by irradiation at longer wavelengths. When both are in a pure phase, anatase generally shows better photocatalytic activity compared to rutile [32] because anatase possesses significantly higher surface area and lower recombination rate of photogenerated charge carriers compared to rutile. Nevertheless, the polymorphic nature of titania film also dictates its photocatalytic activity, and Su et al. [33] concluded that the mixed phases of anatase-rutile at proper amounts showed better photocatalytic activity than pure phase titania by promoting separation of electrons and holes and reducing the opportunity to recombine. However, when rutile titania exceeds, it constitutes an impurity, which has the opposite effect and promotes the recombination of photo-generated holes and electrons [33].

We concluded that 550 °C was the optimum temperature, resulted in TiO_2 film with optimum amount of anatase crystal phase, with high conductivity and photocatalytic properties, and which

facilitates total removal of residual PEG2000 without sacrificing the optimum pore and crystal size which results from the sintering process produced by higher calcination temperatures.

3.4 Effects of the P25 TiO$_2$ loading on the properties of TiO$_2$/SS photo-electrodes

P25 is a commercially popular TiO$_2$ crystal powder, typically consisting of 22% rutile and 78% anatase. With both anatase and rutile in appropriate proportions, P25 has been used successfully in numerous applications. Adding P25 into the sol could increase the quality of the TiO$_2$ film on the SS-mesh substrate, in terms of film crystallinity, porosity and photocatalytic activity (Balasubramanian et al., 2004, 2003; Chen and Dionysiou, 2008, 2006; Ngamsinlapasathian et al., 2005). These properties are discussed in this section.
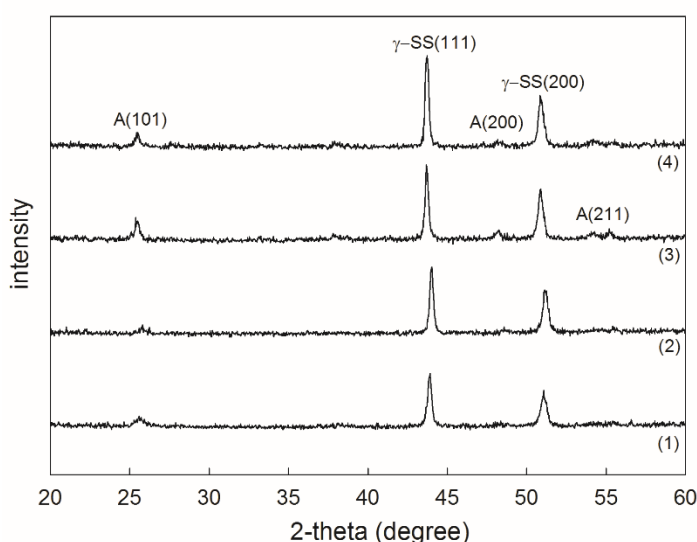

Figure 8. XRD patterns of (1) TiO$_2$/SS (2 dip-coating cycles), (2) P25-30+TiO$_2$/SS, (3) P25-50+TiO$_2$/SS and (4) P25-70+TiO$_2$/SS films.

Patterns 2-4 in Fig. 8 show the XRD patterns of P25-30+TiO$_2$/SS, P25-50+TiO$_2$/SS, and P25-70+TiO$_2$/SS, respectively, and pattern 1 for TiO$_2$/SS is shown here for a comparison purpose. Noted that, the (101) anatase peak intensity of the P25+TiO$_2$/SS electrodes becomes sharper with the P25 loading compared the TiO$_2$/SS, revealing the improvement in crystalline quality of TiO$_2$ on the SS-mesh substrate. These results are similar to those obtained by Chen and Dionysiou [17], excepting that no rutile phase was visible in our study, even though the P25 TiO$_2$ powders originally contain the rutile phase. This might be due to the inclusion of P25 TiO$_2$ nanoparticles by the sol-gel TiO$_2$. Moreover, the XRD patterns show that the higher P25 loading is, the higher SS peaks are observed, suggesting the presence of more microcracks which increase the exposure of the bare SS substrate. The low porosity and relatively high density of the original P25 powders may lower the sol permeability, leading to relatively large internal stresses in the P25+TiO$_2$ film and the generation of microcracks [17].

Table 3. BET surface and total pore volume of various P25+TiO$_2$ films.

P25 loading (g/L)	BET (m^2/g)	Pore volume (cm^3/g)[a]	Porosity (%)[b]
30	0.23	0.84×10^{-2}	3.3
50	0.84	1.59×10^{-2}	6.2
70	2.05	0.92×10^{-2}	3.6

[a]BJH desorption cumulative volume of pores; [b] Based on pore volume and anatase density of the film (3.9 g/cm^3); condition: 1 dip-coating cycle with calcination at 550 °C.
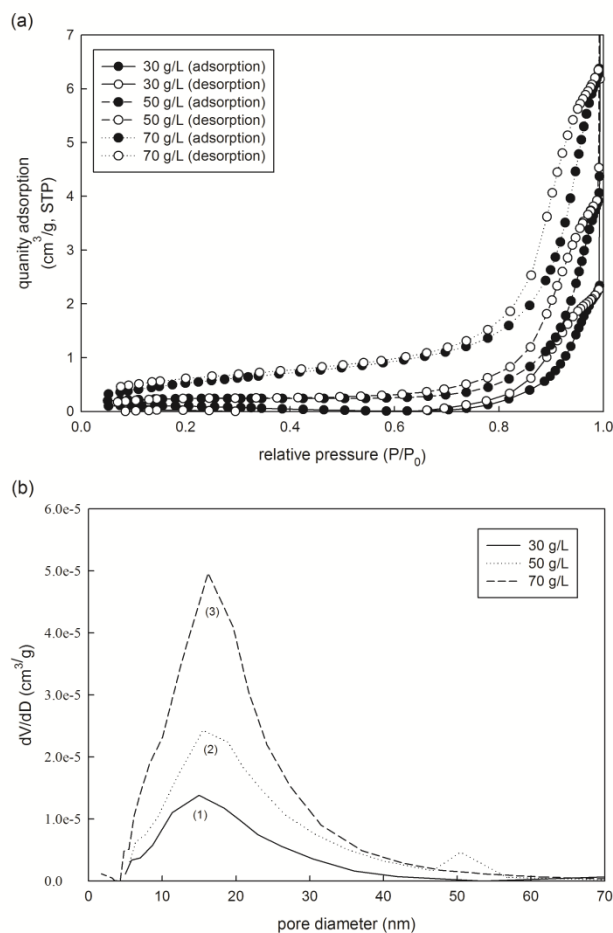
Figure 9. (a) N$_2$ adsorption-desorption isotherms and (b) the corresponding pore size distributions of titania films with P25 content of (1) 30 g/L, P25-30+TiO$_2$, (2) 50 g/L, P25-50+TiO$_2$ and (3) 70 g/L, P25-70+TiO$_2$; condition: 1 dip-coating cycle with calcination at 550 °C.

However, the increase in the P25 dosage in the sol was less pronounced for increasing the film thickness which varied from 3 to 5 μm for the three P25+TiO$_2$/SS electrodes even though a slight increase in the weight of P25+TiO$_2$ films was obtained (i.e., 4.0, 4.4 and 4.8 mg/cm^2 for P25-30+TiO$_2$/SS, P25-50+TiO$_2$/SS, and P25-70+TiO$_2$/SS, respectively). Nevertheless, with only one dip-coating process, the P25+TiO$_2$/SS prepared by the same SGDC method show a much thicker film compared to the TiO$_2$/SS electrode that requires twice dip-coating processes to achieve 1.6 μm in thickness.

Nitrogen adsorption-desorption isotherms for all $P25+TiO_2/SS$ samples in Fig. 9a show the classical Type V adsorption isotherm. Similar to the type IV isotherm, this type is also associated with a mesoporous structure with an exception of weak fluid-wall forces [23]. In comparison with the TiO_2/SS film, the range of pore size distribution for all $P25+TiO_2/SS$ samples is significantly wider, from around 2 to 60 nm (Fig. 9b). The pores characteristics shown in Table 3 demonstrate that the $P25+TiO_2$ films are more porous than the TiO_2 one. The maximum pore volume is achieved when 50 g/L P25 TiO_2 powders are added. It is worth noting that for the $P25-50+TiO_2/SS$ film, other than the mesoporous structure, macropores (i.e., pore diameter > 50 nm) are also formed, possibly caused by the aggregation of P25 nanoparticles within the SGDC-prepared TiO_2 film, which results in the higher total pore volume. When the amount of P25 increases to 70 g/L, the total pore volume decreases (Table 3), indicating that the amount of P25 is too high to complete the P25 nanoparticle inclusion by the SGDC TiO_2 film.

*3.5 Electro-photocatalytic Fenton activity of P25+TiO₂/SS photo-electrodes*

The effect of P25 on the performances of $P25+TiO_2/SS$ electrodes for orange G decolorization via the EPF process is further investigated. After the 3-h EPF reaction, the decolorization efficiencies (478 nm) of all $P25+TiO_2/SS$ electrodes reach 78% (Fig. 10). For the decrease of the 330 nm peak, both $P25-50+TiO_2/SS$ and $P25-70+TiO_2/SS$ electrodes gave 75% removal efficiency, while the removal efficiency for the system using the $P25-30+TiO_2/SS$ electrode only reaches 60%. Different from the case employing the TiO_2/SS electrode, ferrous ions were released in the test solution even in the dark reaction when $P25+TiO_2/SS$ electrodes were employed. This spontaneous dissolution of ferrous ions may be attributed to the microcracks in the TiO_2 films on these $P25-30+TiO_2/SS$ electrodes. The microcracks also cause the significant increase in the ferrous concentration after 3-h EPF reaction; i.e., 2.9, 2.5, and 3.2 mg/L for $P25-30+TiO_2/SS$, $P25-50+TiO_2/SS$, and $P25-70+TiO_2/SS$ electrodes, respectively.

The performance of $P25-TiO_2/SS$ electrode for orange G dye decolorization via EPF was evaluated and compared with PC and EF process, as shown in Fig. 11. The best decolorization (478 nm) efficiency of 78% was achieved when the reaction used EPF driving force. This is opposed to EF and PC, which could only achieve around 71 and 13%, respectively (Fig. 11a). Similarly, naphthalene ring determination at 330 nm resulted in 72, 56, and 14% removal efficiency for EPF, EF and PC, respectively (Fig. 11b). During the EF process, ferrous ion generation increased from 0.9 mg/L after a 1-h dark reaction to 2 mg/L after a 3-h reaction, while measurement of Fe^{2+} during EPF process resulted in similar trends with relatively higher concentrations, showing the increased from 1.7 to 2.5 mg/L after a 1-h dark reaction, until the end of the process.
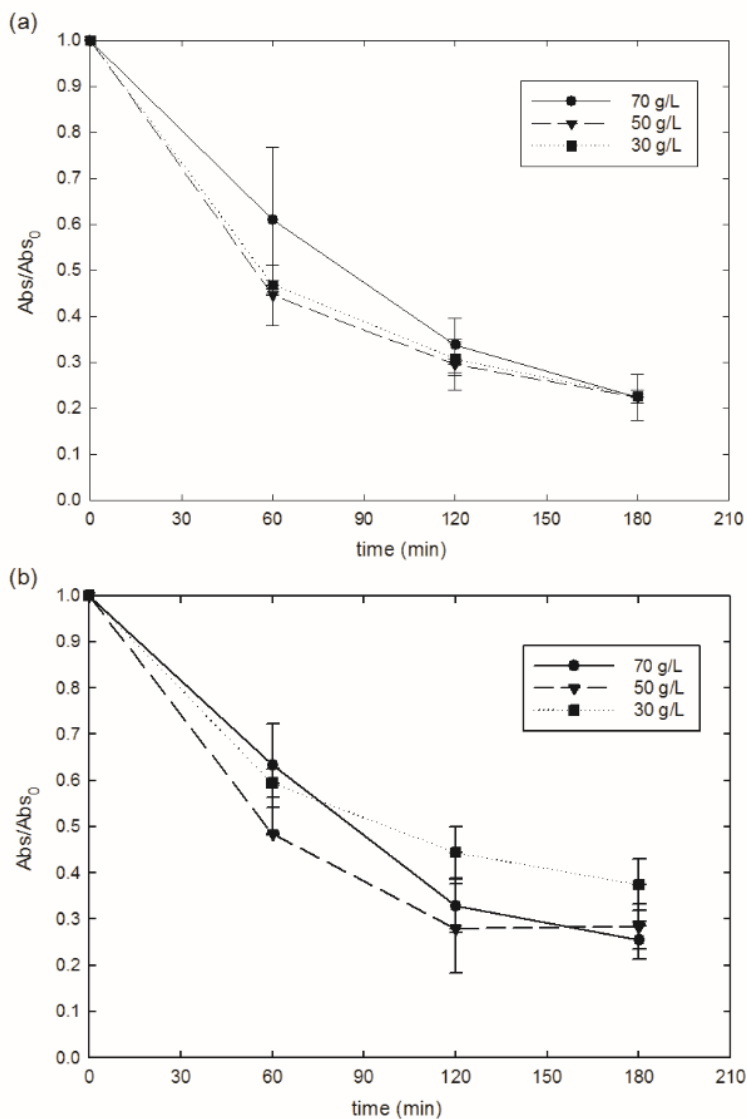
Figure 10. (a) Decolorization (Abs. at 478 nm) and (b) degradation (Abs. at 330 nm) efficiencies of orange G via the EPF process using various P25+TiO$_2$/SS electrodes prepared with P25 concentrations of 30, 50 and 70 mg/L; conditions: orange G dye concentration: 45.2 mg/L, pH: 3, UV light: 0.2 mW/cm^2, potential applied: 1.6 V.

Both TiO$_2$/SS and P25-TiO$_2$/SS electrodes comprise similar decolorization efficiency of around 78%. Nevertheless, it is worth noting that the former needed four dip-coating cycles with film thickness of 7.4 μm, while the P25-TiO$_2$/SS only required one dip-coating process giving a 3-5 μm thick film to achieve the same result. Therefore, P25-modified SGDC method considerably enhanced the efficiency of TiO$_2$ film fabrication, especially for water treatment application.
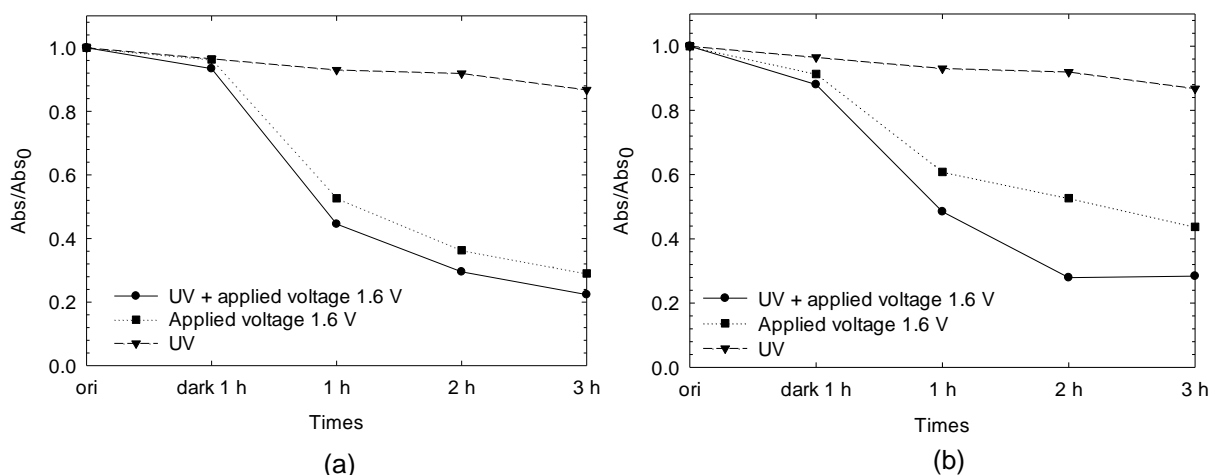
Figure 11. Decolorization efficiency: (a) Abs. at 478 nm and (b) Abs. at 330 nm of P25+TiO$_2$/SS operated under different AOPs processes (PEF, EF and PC); conditions: orange G dye concentration: 45.2 mg/L, pH: 3, UV light: 0.2 mW/cm^2, potential applied: 1.6 V.
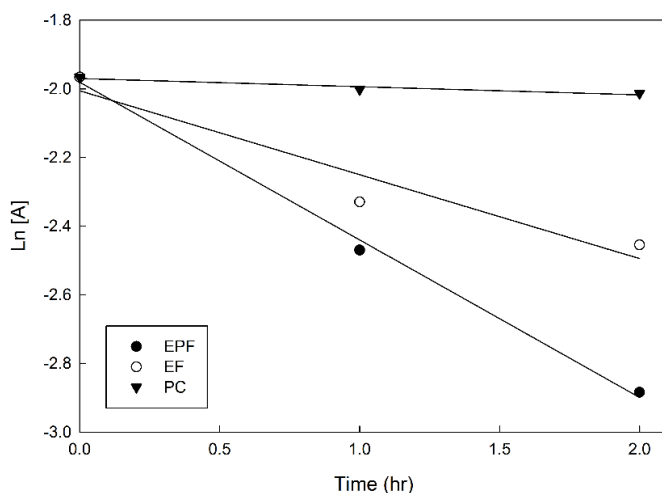
Figure 12. Pseudo first-order kinetics of orange G decolorization via PEF, EF and PC (Abs. at 330 nm)

Figure 12 shows that for the first two hours after dark reaction the decolorization of orange G follow pseudo first-order kinetics [36]. Reaction rate coefficient for PC, EF and PEF were $k_{PC} = 0.024$/h, $k_{EF} = 0.244$/h, $k_{EPF} = 0.997$/h respectively evidence that degradation via electro-photocatalytic Fenton reaction occurs much faster than photocatalytic and electro-Fenton process.

4. CONCLUSIONS

This work successfully developed novel TiO$_2$ film electrodes for a robust photo-electrochemical process. The high surface area of the TiO$_2$ film electrodes resulting from the

mesoporous structure of the film provides large active sites for the wastewater to interact with the catalyst, and thus to undergo degradation efficiently. The higher PEG2000 concentrations resulted in more porous film, while increasing the number of dip-coating cycles significantly increased the film thickness. The calcination temperature played an essential role in determining the crystallinity of the TiO_2 film. Modifying the SGDC method by adding P25 powder enhances TiO_2 immobilization and also induces microcracks in the film at the same time. The release of ferrous ions from SS-mesh substrate promoted by these microcracks facilitates the electro-photocatalytic Fenton reaction that causes the orange G dye decolorization to occur much faster compared to photocatalytic and electro-Fenton process. The findings of this work implied that an SGDC method modified by adding P25 powder during sol-gel process substantially enhances the efficiency of TiO_2 film fabrication.

References

1.   J.C. Diogo, A. Morao, A. Lopes, *Environ. Prog. Sustain. Energy* 30 (2011) 399–408.
2.   S. Garcia-Segura, S. Dosta, J.M. Guilemany, E. Brillas, *Appl. Catal. B Environ.* 132-133 (2013) 142–150.
3.   C.A. Martínez-Huitle, E. Brillas, *Appl. Catal. B Environ.* 87 (2009) 105–145.
4.   P. V. Nidheesh, R. Gandhimathi, *Desalination* 299 (2012) 1–15.
5.   A. El-Ghenymy, R.M. Rodríguez, C. Arias, F. Centellas, J.A. Garrido, P.L. Cabot, E. Brillas, *J. Electroanal. Chem.* 701 (2013) 7–13.
6.   C. Flox, S. Ammar, C. Arias, E. Brillas, A.V. Vargas-Zavala, R. Abdelhedi, *Appl. Catal. B Environ.* 67 (2006) 93–104.
7.   Y.-H. Huang, H.-T. Su, L.-W. Lin, *J. Environ. Sci.* 21 (2009) 35–40.
8.   M. Zarei, A.R. Khataee, R. Ordikhani-Seyedlar, M. Fathinia, *Electrochim. Acta* 55 (2010) 7259–7265.
9.   K. Hofstadler, R. Bauer, S. Novalic, G. Heisler, *Environ. Sci. Technol.* 28 (1994) 670–4.
10.   G.K. Mor, K. Shankar, M. Paulose, O.K. Varghese, C.A. Grimes, *Nano Lett.* 5 (2005) 191–5.
11.   G. Sberveglieri, *Sensors Actuators B Chem.* 23 (1995) 103–109.
12.   S. Berger, A. Ghicov, Y.-C. Nah, P. Schmuki, *Langmuir* 25 (2009) 4841–4.
13.   A. S. El-Kalliny, S.F. Ahmed, L.C. Rietveld, P.W. Appel, *Drink. Water Eng. Sci. Discuss.* 7 (2014) 59–94.
14.   C.-H. Su, C.-C. Hu, Y.-C.C. Sun, Y.-C. Hsiao, *J. Taiwan Inst. Chem. Eng.* (2015).
15.   Y. Xin, H. Liu, L. Han, Y. Zhou, *J. Hazard. Mater.* 192 (2011) 1812–8.
16.   X. Chen, S.S. Mao, *Chem. Rev.* 107 (2007) 2891–959.
17.   Y. Chen, D.D. Dionysiou, *Appl. Catal. B Environ.* 62 (2006) 255–264.
18.   G. Balasubramanian, D.D. Dionysiou, M.T. Suidan, V. Subramanian, I. Baudin, J.M. Laîné, *J. Mater. Sci.* 38 (2003) 823–831.
19.   Y. Chen, D.D. Dionysiou, *Appl. Catal. B Environ.* 80 (2008) 147–155.
20.   T. Miki, K. Nishizawa, K. Suzuku, K. Kato, K. Suzuki, K. Kato, *J. Mater. Sci.* 39 (2004) 699–701.
21.   H. Choi, E. Stathatos, D.D. Dionysiou, *Thin Solid Films* 510 (2006) 107–114.

22.   L. Zhang, *Appl. Catal. B Environ.* 40 (2003) 287–292.
23.   P.B. Balbuenat, K.E. Gubbins, *Langmuir* 9 (1993) 1801–1814.
24.   J. Yu, G. Dai, B. Cheng, *J. Physic Chem. C* 114 (2010) 19378–19385.
25.   Y. Chen, S. Lunsford, D.D. Dionysiou, *Thin Solid Films* 516 (2008) 7930–7936.
26.   E. Pajootan, M. Arami, M. Rahimdokht, *Ind. Eng. Chem. Res.* 53 (2014) 16261–16269.
27.   J.-H. Sun, S.-H. Shi, Y.-F. Lee, S.-P. Sun, *Chem. Eng. J.* 155 (2009) 680–683.
28.   R. Bauer, Catal. Today 53 (1999) 131–144.
29.   Y. Juang, Y. Liu, E. Nurhayati, N.T. Thuy, C. Huang, C.-C. Hu, *Chemosphere* 144 (2016)
       2462–2468.
30.   A.Y. Mounia, Z. Djilali, *Desalin. Water Treat.* (2014) 1–12.
31.   R.-R. Raminta, R. Saule, V. Snitka, G. Saulis, *IEEE Trans. Plasma Sci.* 42 (2014) 249–254.
32.   T. Luttrell, S. Halpegamage, J. Tao, A. Kramer, E. Sutter, M. Batzill, *Sci. Rep.* 4 (2014) 4043.
33.   Y. Su, X. Zhang, M. Zhou, S. Han, L. Lei, *J. Photochem. Photobiol. A Chem.* 194 (2008) 152–
       160.
34.   G. Balasubramanian, D. Dionysiou, M. Suidan, I. BaudinN, J. Laine, *Appl. Catal. B Environ.* 47
       (2004) 73–84.
35.   S. Ngamsinlapasathian, T. Sreethawong, Y. Suzuki, S. Yoshikawa, *Sol. Energy Mater. Sol.
       Cells* 86 (2005) 269–282.
36.   E. Brillas, B. Boye, I. Sirés, J.A. Garrido, R.M. Rodríguez, C. Arias, P.-L. Cabot, C.
       Comninellis, *Electrochim. Acta* 49 (2004) 4487–4496.